A Comparative Study of Hydroxyapatite- and Alumina-Based Catalysts in Dry Reforming of Methane

Bruna Rêgo de Vasconcelos, Doan Pham Minh, Emmanuel Martins, Alain Germeau, Patrick Sharrock, Ange Nzihou

Bruna Rego de Vasconcelos[1,2]
Doan Pham Minh[1,3,*]
Emmanuel Martins[4]
Alain Germeau[4]
Patrick Sharrock[1]
Ange Nzihou[1]

A Comparative Study of Hydroxyapatite- and Alumina-Based Catalysts in Dry Reforming of Methane

The dry reforming of methane over hydroxyapatite- and alumina/magnesia (commercial Pural MG 30)-supported nickel catalysts was investigated. The catalytic performance of the catalysts prepared with fresh supports highly depended on the basicity, the metal-support interaction, and the metal particle size. Calcination of the supports at 1200 °C for 5 h made the catalysts less active because of specific surface area reduction and basicity destruction. However, this treatment allowed avoiding any further catalyst deactivation by thermal sintering and maintained excellent catalytic stability over 300 h of time-on-stream. These tests under simulated industrial conditions (high contact time and long time-on-stream) showed the competitiveness of the prepared catalysts in this important catalytic process.

Keywords: Carbon dioxide, Dry reforming of methane, Hydroxyapatite, Nickel-based catalysts, Simulated industrial conditions

1 Introduction

The reaction of dry reforming of methane (DRM; Eq. 1) has been intensively studied in the last decades since it allows converting two main greenhouse gases (CH_4 and CO_2) into syngas (CO and H_2), which is a key building block for the production of fuels and chemicals. Despite the economic and environmental interest, this process has not yet achieved the large industrial scale. One of the major challenges preventing the commercialization of DRM (Eq. 1) is the fast catalyst deactivation by coke deposition as well as by thermal sintering. Coke deposition is generally caused by carbon-forming side reactions, such as the Boudouard reaction (Eq. 2), methane cracking (Eq. 3), and reverse carbon gasification (Eq. 4) [1, 2].

Dry reforming of methane:

$$CH_4 + CO_2 \rightleftharpoons 2H_2 + 2CO \quad (1)$$

Boudouard reaction:

$$2CO \rightleftharpoons C_{(s)} + CO_2 \quad (2)$$

Methane cracking:

$$CH_4 \rightleftharpoons C_{(s)} + 2H_2 \quad (3)$$

Reverse carbon gasification:

$$CO + H_2 \rightleftharpoons C_{(s)} + H_2O \quad (4)$$

In fact, coke deposits are usually in whisker form, which has high mechanical strength. Once they grow on the catalyst surface, the catalyst pellets will break and fractionate. This will lead to a breakdown of the process due to an increase of the pressure drop inside the reactor [3, 4]. Also, as the DRM reaction is thermodynamically favored at high temperatures [2], sintering of both the support and the active phase may occur, provoking irreversible catalyst deactivation due to the reduction of the specific surface area of the catalyst and the total amount of active sites [5, 6]. The strategy to overcome catalytic deactivation is to optimize the operating conditions in association with the use of a performing catalyst, which must withstand the harsh reaction conditions for long times-on-stream (TOS) [3, 7].

Nickel-based catalysts are industrially preferred due to the lower cost of nickel in comparison to noble metals [8]. Thus, designing a performing catalyst consists in the development of a suitable catalyst support having the required properties for the DRM process, such as the ability of high metal dispersion, strong metal-support interaction, controlled acido-basicity, and high resistance to thermal sintering. In our previous work [9], hydroxyapatite ($Ca_{10}(PO_4)_6(OH)_2$), hereafter named Ca-HA,

[1]Dr. Bruna Rego de Vasconcelos, Dr. Doan Pham Minh, Prof. Dr. Patrick Sharrock, Prof. Dr. Ange Nzihou,
doan.phamminh@mines-albi.fr
Université de Toulouse, IMT Mines Albi, UMR CNRS 5302, Centre RAPSODEE, Campus Jarlard, 81013 Albi cedex 09, France.

[2]Dr. Bruna Rego de Vasconcelos
Biomass Technology Laboratory, Department of Chemical and Biotechnological Engineering, Université de Sherbrooke, Sherbrooke, Québec J1K 2R1, Canada.

[3]Dr. Doan Pham Minh
Institute of Research and Development, Duy Tan University, Da Nang 550000, Vietnam.

[4]Emmanuel Martins, Dr. Alain Germeau
PRAYON S.A., rue J. Wauters, 144, 4480 Engis, Belgium.

has been shown to be a new promising support for the DRM reaction, which responds to different criteria required of a DRM catalyst. This work continues to explore these catalysts and was focused on the influence of support calcination, in order to avoid any further thermal sintering. Catalytic tests were done under simulated industrial conditions with high contact time and for prolonged TOS. The performance of these catalysts was compared with that of alumina/magnesia-supported nickel catalysts, as a reference.

2 Materials and Methods

2.1 Catalyst Preparation and Characterization

Two hydroxyapatites, Ca-HA1 and Ca-HA2, produced and provided by our industrial partner (PRAYON, Belgium) were tested as catalyst support. Pural MG 30 (30 wt % MgO and 70 wt % Al_2O_3), a commercial support from Sasol, was used as reference. In fact, a nickel-based catalyst prepared with this support has been reported as one of the most efficient catalysts in the DRM reaction for syngas production [10]. All the supports were employed in two forms: as received (named as Ca-HA1, Ca-HA2, 30MgAl) and after calcination at 1200 °C for 5 h under air (named as Ca-HA1_S, Ca-HA2_S, 30MgAl_S). The objective of this calcination was to stabilize the supports and avoid eventual catalyst deactivation by support thermal sintering. Data related to this thermal treatment was reported elsewhere [11]. The catalysts were prepared by the incipient wetness impregnation method. The supports were impregnated with an aqueous solution of $Ni(NO_3)_2{\cdot}6H_2O$ (Fisher Scientific, > 98 wt %) to reach a theoretical nickel loading of 5.7 wt %. After impregnation, the powder was dried at 105 °C. The catalysts are referred to as Ni/Ca-HA1, Ni/Ca-HA2, Ni/30MgAl, Ni/Ca-HA1_S, Ni/Ca-HA2_S, and Ni/30MgAl_S.

Fresh and spent supports and catalysts were characterized by various physicochemical analyses including: nitrogen adsorption-desorption, carbon dioxide temperature-programmed desorption (CO_2-TPD), inductively coupled plasma-optical emission spectroscopy (ICP-OES), X-ray diffraction (XRD), and temperature-programmed reduction (TPR).

Details of the apparatus used and the operational conditions can be found in the Supplementary Information, Sect. S1.

2.2 Catalytic Test

The DRM reaction was carried out in a fixed-bed tubular reactor (8 mm i.d.). For each test, 340 mg of dried catalyst was diluted two times with non-porous and inert alumina powder, which was then placed at the center of the reactor, between two layers of the same alumina. The pressure drop in the reactor was 160 000 Pa. The reaction temperature was controlled by a thermocouple placed at the center of the catalyst bed. The catalyst was reduced in situ at 700 °C for 2 h under 4 vol. % of H_2 in N_2 (flow rate of 70 $mL_N\,min^{-1}$; mL_N = normalized milliliter). Then, the DRM reaction was started at 700 °C by switching to a gas mixture containing 20 % CH_4, 20 % CO_2, and 60 % N_2 (vol. %) at 90 $mL_N\,min^{-1}$, with a weight hourly space velocity (*WHSV*) of 20.3 h^{-1}. For the tests under simulated industrial conditions, 440 mg of dried catalyst was used and the feeding flow rate was kept at 90 $mL_N\,min^{-1}$, reaching a *WHSV* value of 15.7 h^{-1}. The reaction was performed for long TOS of 300 h. A silica gel tube was used as water trap at the reactor outlet for quantification of the water formed during the reaction. A gas counter was also used for the measurement of the total gas flow rate at the reactor outlet. This measurement was crucial for the calculation of the reaction conversion and selectivity. In fact, the DRM led to a change of the outlet gas flow rate compared to the inlet gas flow rate. Details of the catalytic reactor can be found elsewhere [9]. Gas products were analyzed by a μ-GC A3000 (Agilent) equipped with a thermal conductivity detector (TCD). From the μ-GC analysis, the conversion of CH_4 and CO_2, the selectivity of conversion into H_2, CO, H_2O, and solid carbon ($C_{(s)}$), and the molar ratio of H_2/CO, which were defined in our previous work [9], could be determined.

3 Results and Discussion

3.1 Characterization

The characterization results of the supports and catalysts are detailed in the Supporting Information (Sect. S2). Briefly, Ca-HA1 was a non-porous material with a low specific surface area, while Ca-HA2 and 30MgAl contained mesopores with higher specific surface area (Tab. 1). They are all basic supports, but the density of the basic sites of 30MgAl was much higher than that of Ca-HA2 and Ca-HA1, explained by the high Mg content. CO_2-TPD evidenced the simultaneous presence of weak, medium, and strong basic sites. These sites were mostly destroyed by the calcination at 1200 °C because of the reduction of the specific surface area (Tab. 1).

Nickel oxide particles could be found in the hydroxyapatite-supported catalysts, highlighted by the XRD results (Supporting Information Fig. S3a, b). On the other hand, a solid solution ($Mg_{0.4}Ni_{0.6}O$) was formed with the 30MgAl and 30MgAl_S supports (Supporting Information Fig. S3c). These results were confirmed by transmission electron microscopy (TEM) analysis. Large nickel-based particles of 100–200 nm were observed for Ni/Ca-HA1 and Ni/Ca-HA1_S, while smaller particles of 10–20 nm were observed for Ni/Ca-HA2 and Ni/Ca-HA2_S (Supporting Information Fig. S4). No visible nickel-based particles could be observed for Ni/30MgAl and Ni/30MgAl_S because of the formation of $Mg_{0.4}Ni_{0.6}O$ solid solution instead of nickel oxide particles (Supporting Information Fig. S4). Finally, TPR highlighted the reduction of nickel species of the prepared catalysts below 500 °C (Supporting Information Fig. S5).

3.2 Catalytic Test

Fig. 1 shows the comparable initial catalytic activities of the catalysts prepared with fresh supports. However, their catalytic behavior was different from one another within 50 h of TOS. Ni/30MgAl showed the best catalytic performance. The CH_4

Table 1. Physicochemical properties of the supports and fresh catalysts.

Sample	Textural characterization		ICP-OES	CO_2-TPD
	S_{BET} [m^2g^{-1}]	V_p [cm^3g^{-1}]	Ni content [wt %]	Total basicity [mmol g^{-1}]
Ca-HA1	7	0	n.m.	0.07
Ca-HA2	60	0.072	n.m.	0.23
30MgAl	148	0.17	n.m.	1.46
Ca-HA1_S	< 3	0	n.m.	0
Ca-HA2_S	< 3	0	n.m.	0
30MgAl_S	< 3	0	n.m.	0.05
Ni/Ca-HA1	6	n.m.	5.0	n.m.
Ni/Ca-HA2	57	n.m.	5.0	n.m.
Ni/30MgAl	94	n.m.	6.0	n.m.
Ni/Ca-HA1_S	< 3	n.m.	4.0	n.m.
Ni/Ca-HA2_S	< 3	n.m.	5.0	n.m.
Ni/30MgAl_S	< 3	n.m.	5.7	n.m.

n.m., Not measured.

and CO_2 conversions were perfectly stable at around 85 % during 50 h of TOS. The H_2 and CO selectivities were also kept constant at 90 % and 98 %, respectively. As a consequence of the high syngas selectivity, very low H_2O and $C_{(s)}$ selectivity was observed (Supporting Information Fig. S6). The performance of the Ni/Ca-HA2 catalyst was similar to that of the Ni/30MgAl catalyst. The catalytic performance of these two catalysts can be explained by their physicochemical properties. They contained small Ni particles (TEM analysis; Supporting Information Fig. S4), which are known to be efficient in preventing carbon deposition [12–16]. Ni/30MgAl was slightly more active than Ni/Ca-HA2 because of its higher density of basic sites, which favors CO_2 adsorption and carbon gasification, its higher

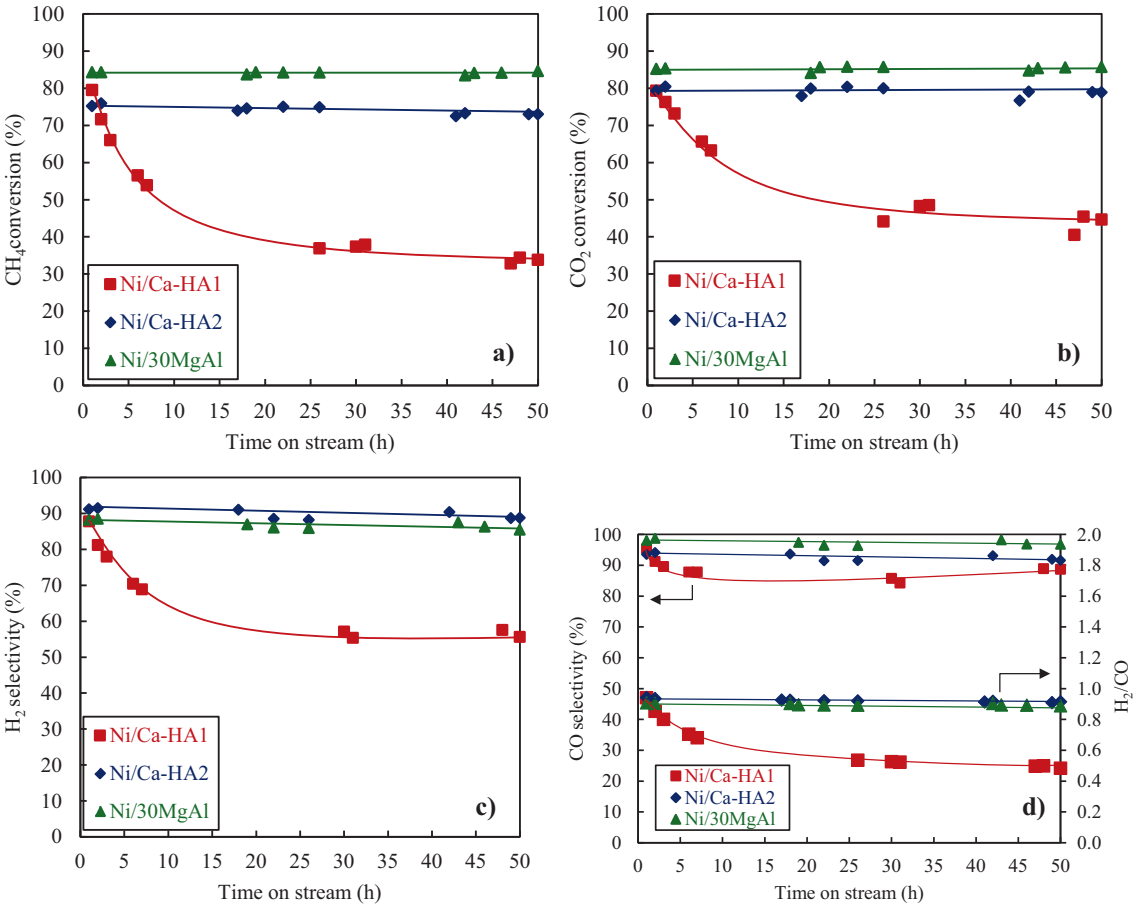

Figure 1. Catalytic performance of the catalysts prepared with fresh supports. Reaction conditions: 700 °C, 160 000 Pa, m_{cat} = 340 mg, *WHSV* = 20.3 h^{-1}.

metal dispersion (particles invisible under TEM), and its stronger metal-support interaction due to the formation of a NiO-MgO solid solution (TPR peak at higher temperature; Supporting Information Fig. S5a).

The CH_4 conversions of both catalysts were slightly smaller than the thermodynamic limit, while the CO_2 conversions were higher than the thermodynamic limit, which is around 67 % according to Jafarbegloo et al. [17]. The presence of basic sites in both catalysts favored the CO_2 adsorption and conversion, which explains the difference between the experimental results and the thermodynamic calculation.

Differently from the other two catalysts, Ni/Ca-HA1 had a strong deactivation within 50 h of TOS. This could be related to its large Ni-based particles as evidenced by TEM analysis (Supporting Information Fig. S4). In fact, large Ni-based particles favor carbon deposition [12–16].

Fig. 2 shows the results obtained with the catalysts prepared with calcined supports at low contact time (*WHSV* 20.3 h^{-1}). For the Ni/30MgAl_S catalyst, the initial CH_4 conversion was 55 % and decreased to 34 % during the test, while the CO_2 conversion decreased from 55 % to 38 %. The H_2 and CO selectivities were kept constant at around 85 % (Supporting Information Fig. S7). Very low H_2O selectivity was observed, but the $C_{(s)}$ selectivity was above 10 % during the test (Supporting Information Fig. S7).

The Ni/Ca-HA1_S and Ni/Ca-HA2_S catalysts had similar catalytic behaviors. They were initially active but catalytic deactivation quickly took place during the first day of the test. In parallel, the selectivity for the desired products, H_2 and CO, strongly decreased and that for undesired products, H_2O and $C_{(s)}$, strongly increased. These results evidence the occurrence of the reverse water-gas shift reaction, reverse carbon gasification (Eq. 4), and methane cracking (Eq. 3), which favor the formation of H_2O and $C_{(s)}$, and caused the catalyst deactivation.

It is worth noting that the catalysts prepared with calcined supports showed lower catalytic performance than the catalysts prepared with fresh supports, despite the similarities in the nickel particle sizes. In fact, the calcination at 1200 °C destroyed the specific surface area and the density of the basic sites of the supports (Tab. 1), which are essential for CO_2 adsorption and consequent gasification of the carbon deposits [18].

The support calcination led to strong catalyst deactivation during the test (Fig. 2), as expected. However, catalysts prepared with calcined supports have the advantage of avoiding further thermal sintering. As previously stated, one of the approaches to deploy the DRM process at the industrial scale is to determine the operating conditions in combination with a suitable catalyst [3, 7]. Generally, increasing the contact time (decreasing the *WHSV*) allows increasing the CH_4 and CO_2 conversions and so limiting side reactions such as CH_4 cracking (Eq. 3) [19]. Figs. 3 and 4 show the results obtained with Ni/Ca-HA1_S, Ni/Ca-HA2_S, and Ni/30MgAl_S at high contact time for prolonged TOS (300 h).

The Ni/Ca-HA2_S catalyst presented the best catalytic performance under the test conditions used. The initial CH_4 and CO_2 conversions were about 80 %; however, they progressively decreased during the test and reached about 60 % at 300 h of TOS. The H_2 selectivity decreased from 90 % to around 65 %, while the CO selectivity was kept constant around 85 % during the test. Low H_2O and $C_{(s)}$ selectivity was observed. This result suggests the occurrence of the reverse water-gas shift reaction, which consumes H_2 and CO_2 to produce H_2O and CO. Also, the formation of $C_{(s)}$ suggests the occurrence of the carbon-forming reactions, such as methane cracking (Eq. 3). Fig. 5 illustrates TEM images of the spent catalyst Ni/Ca-HA2_S. The sizes of the nickel particles on the spent catalyst were around 10–20 nm, which indicates that no thermal sintering of the active phase took place during the 300 h of reaction. For comparison, the average deactivation rate is defined in Eq. (5), and the results are shown in Tab. 2. The low average deactivation rate of this catalyst (0.17 % h^{-1} at 50 h of TOS and 0.07 % h^{-1} at 300 h of TOS) can be explained by the formation of carbon nanotubes (CNT) and carbon nanofibers (CNF) on the surface of this catalyst, instead of amorphous carbon species, which cover the catalyst surface and lead to catalyst deactivation. Moreover, CNT and CNF have been reported as good catalyst supports for the DRM reaction [20, 21]. Hence, when they are

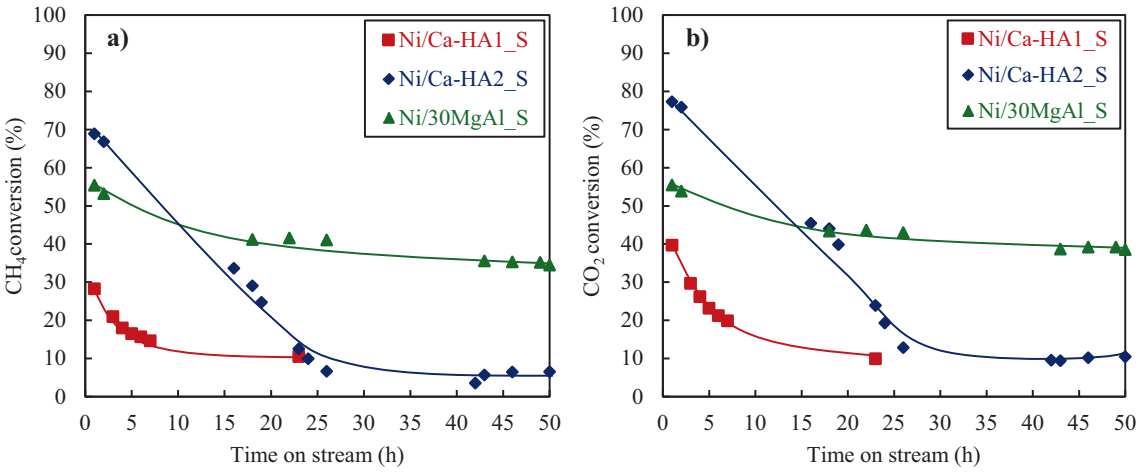

Figure 2. Catalytic performance of the catalysts prepared with calcined supports at low contact time. Reaction conditions: 700 °C, 160 000 Pa, m_{cat} = 340 mg, *WHSV* = 20.3 h^{-1}.

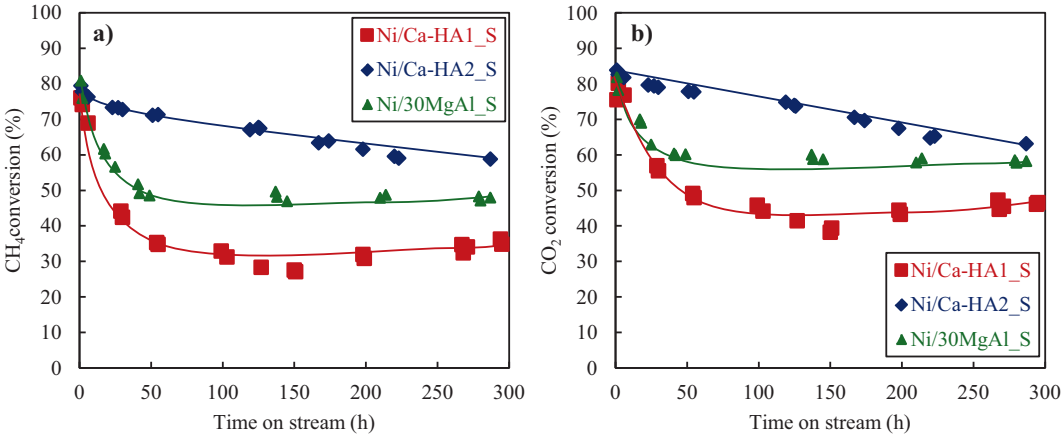

Figure 3. CH_4 and CO_2 conversions at high contact time of the catalysts prepared with calcined supports. Reaction conditions: 700 °C, 160 000 Pa, m_{cat} = 340 mg, *WHSV* = 20.3 h^{-1}.

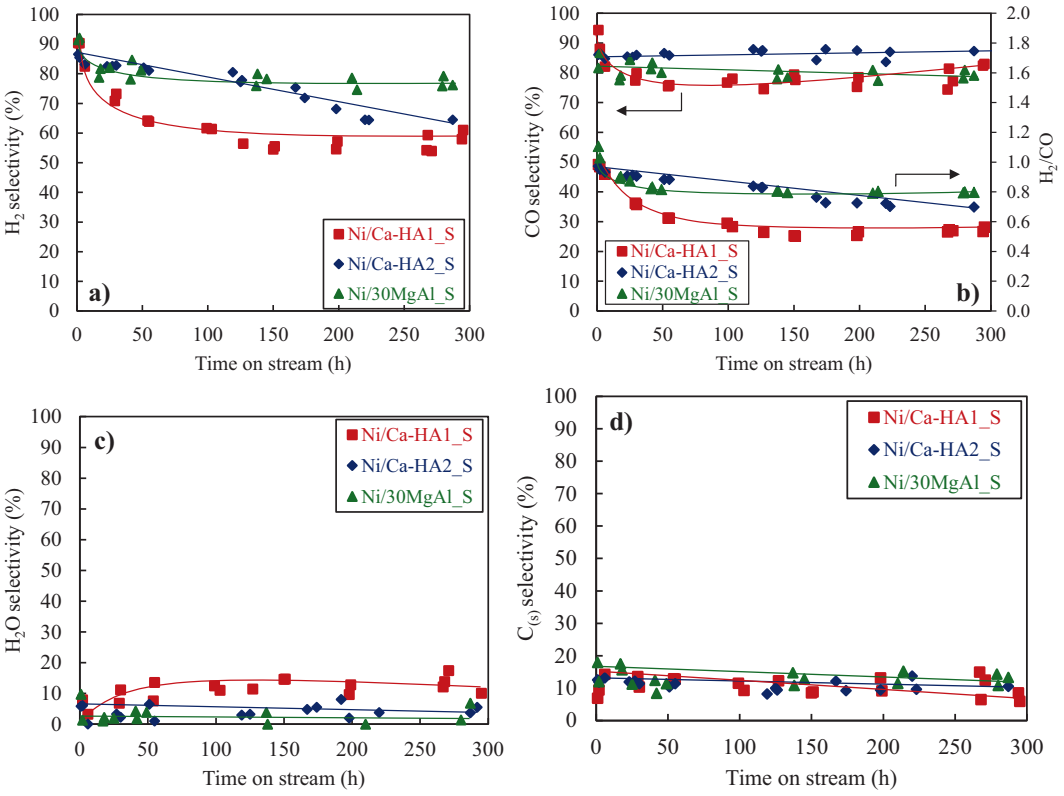

Figure 4. Selectivity for certain products at high contact time of the catalysts prepared with calcined supports. Reaction conditions: 700 °C, 160 000 Pa, m_{cat} = 440 mg, *WHSV* = 15.7 h^{-1}.

formed during the DRM reaction, they probably become part of the catalytic system.

$$\text{Average deactivation rate } (\%h^{-1}) = \frac{CH_4\text{conversion after 1h of TOS} - CH_4\text{conversion after X h}}{X - 1} \quad (5)$$

The Ni/Ca-HA1_S catalyst showed similar initial catalytic activity compared to Ni/Ca-HA2_S. However, CH_4 and CO_2 conversion and the selectivity for the main products (H_2 and CO) strongly decreased within the first 50 h of TOS, before stabilization. In parallel, high selectivity for the by-products, such as water, was observed. As previously explained, the decrease in H_2 selectivity was attributed to the reverse water-gas shift reaction. Fig. 6 shows a TEM image of the Ni/Ca-HA1_S catalyst after 300 h of TOS. The Ni particle sizes on the spent catalyst (which was up to 200 nm) were similar to those of the fresh catalysts, which means that no thermal sintering of the active

Table 2. Deactivation rates of the studied catalysts.

Catalyst	Deactivation rate [% h^{-1}] at TOS = 50 h	Deactivation rate [% h^{-1}] at TOS = 300 h
Ni/Ca-HA1_S	0.77	0.14
Ni/Ca-HA2_S	0.17	0.07
Ni/30MgAl_S	0.67	0.12

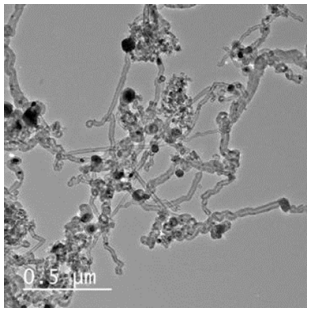

Figure 5. TEM images of the spent catalyst Ni/Ca-HA2_S after 300 h of TOS at 700 °C.

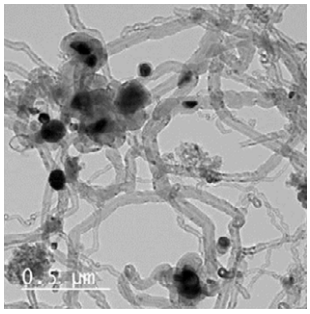

Figure 6. TEM images of the spent catalyst Ni/Ca-HA1_S after 300 h of TOS at 700 °C.

phase took place. The deactivation of the catalyst was related to the carbon deposition in core-shell form, which prevents access of the reactants to the Ni-based particles, which explains the much higher deactivation rate of this catalyst (0.77 % h^{-1} at 50 h of TOS and 0.14 % h^{-1} at 300 h of TOS), much higher than that of Ni/Ca-HA2_S (Tab. 2).

The catalytic behavior of Ni/30MgAl_S was different from those of Ni/Ca-HA1_S and Ni/Ca-HA2_S. After an initial deactivation of about 30 % in CH_4 conversion and 20 % in CO_2 conversion within 50 h of TOS, the activity of this catalyst was relatively stable. The H_2 and CO selectivity slightly decreased from 90 % to 80 % within the first hours of reaction. Then, it was kept constant at 80 %. The H_2O selectivity was very low during 300 h of TOS. Initially, the $C_{(s)}$ selectivity was around 20 % and then decreased to around 10 %. The high carbon selectivity at the beginning of the test explains the high initial deactivation rate of this catalyst (Tab. 2). The low selectivity for conversion into water and the stability of this catalyst after 50 h of TOS indicate the occurrence of the carbon gasification reaction (Eq. 4), where the carbon deposit reacts with the water to produce syngas. Fig. 7 shows a TEM image of the spent catalyst

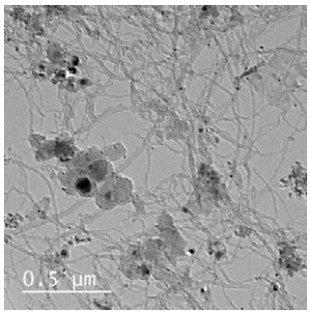

Figure 7. TEM images of the spent catalyst Ni/30MgAl_S after 300 h of TOS at 700 °C.

Ni/30MgAl_S after 300 h of TOS. In contrast to the fresh catalyst, Ni particles of sizes up to 100 nm could be visualized, which indicated that thermal sintering of the nickel particles and/or decomposition of the $Mg_{0.4}Ni_{0.6}O$ solid solution occurred during the reaction. As highlighted by the TPR analysis (Supporting Information Fig. S5), the calcination led to a shift of the TPR peak to a lower temperature, indicating a weaker metal-support interaction of Ni/30MgAl_S compared to Ni/30MgAl. Moreover, carbon deposits under CNT/CNF and core-shell forms were detected. Both the sintering of the active phase and carbon deposition provoked the initial catalyst deactivation of this catalyst. The average deactivation rate of this catalyst was also higher than that of Ni/Ca-HA2_S. It is worth noting that the performance of the Ni/Ca-HA_2 catalyst kept decreasing during the test without reaching stabilization. Despite the fact that this catalyst presented the best catalytic performance during 300 h of TOS (which is considerably longer than initial industrial validation tests that usually lasted for 100 h), its performance might eventually reach similar values to that of the Ni/30MgAl_S. Hence, the next step of the investigation should be to first evaluate their performances over a longer TOS (350 h, for example), to verify if the catalysts reach similar performances and to better investigate why the Ni/Ca-HA_2 catalyst presents lower deactivation rates than the Ni/30MgAl_S catalyst.

4 Conclusions

Nickel-supported catalysts prepared with two hydroxyapatites (Ca-HA1 and Ca-HA2) and a commercial support (Pural MG30) were investigated in the DRM reaction. The two catalysts prepared with the fresh supports, Ni/30MgAl and Ni/Ca-HA2, were the most active and stable during 50 h of TOS. This is explained by the high density of basic sites of the supports (up to 1.46 mmol g^{-1}), the high specific surface area (up to 94 m^2g^{-1}), small Ni particles (< 20 nm), and strong metal-support interactions.

The catalysts prepared with calcined supports had lower catalytic activity compared to those prepared with fresh supports. This was related to the reduction of the specific surface area and the decrease of the basic site density of the supports. By combination with operation condition control (increase of the contact time), the catalytic activity of these catalysts could be stabilized after an initial deactivation. The Ni/Ca-HA2_S

catalyst showed the lowest deactivation rate after 300 h of TOS and should not present any further risk of thermal sintering. This can open a new perspective for deploying DRM on a large scale.

Acknowledgments

The authors gratefully thank PRAYON for financial support, and colleagues at RAPSODEE laboratory for technical help.

The authors have declared no conflict of interest.

Abbreviations

CO_2-TPD	carbon dioxide temperature-programmed desorption
DRM	dry reforming of methane
ICP-OES	inductively coupled plasma-optical emission spectroscopy
TEM	transmission electron microscopy
TPR	temperature-programmed reduction
WHSV	weight hourly space velocity
XRD	X-ray diffraction

References

[1] A. Abdulrasheed, A. A. Jalil, Y. Gambo, M. Ibrahim, H. U. Hambali, M. Y. S. Hamid, *Renewable Sustainable Energy Rev.* **2019**, *108*, 175. DOI: https://doi.org/10.1016/j.rser.2019.03.054

[2] N. A. K. Aramouni, J. G. Touma, B. A. Tarboush, J. Zeaiter, M. N. Ahmad, *Renewable Sustainable Energy Rev.* **2018**, *82*, 2570. DOI: https://doi.org/10.1016/j.rser.2017.09.076

[3] P. M. Mortensen, I. Dybkjær, *Appl. Catal., A* **2015**, *495*, 141. DOI: https://doi.org/10.1016/j.apcata.2015.02.022

[4] S. Helveg, P. L. Hansen, *Catal. Today* **2006**, *111 (1/2)*, 68. DOI: https://doi.org/10.1016/j.cattod.2005.10.019

[5] H. S. A. de Sousa, A. N. da Silva, A. J. R. Castro, A. Campos, J. M. Filho, A. C. Oliveira, *Int. J. Hydrogen Energy* **2012**, *37 (17)*, 12281. DOI: https://doi.org/10.1016/j.ijhydene.2012.05.151

[6] H. Ay, D. Üner, *Appl. Catal., B* **2015**, *179*, 128. DOI: https://doi.org/10.1016/j.apcatb.2015.05.013

[7] R. J. Farrauto, J. N. Armor, *Appl. Catal., A* **2016**, *527*, 182. DOI: https://doi.org/10.1016/j.apcata.2016.09.008

[8] S. Wang, G. Q. Lu, G. J. M. Millar, *Energy Fuels* **1996**, *10 (4)*, 896. DOI: https://doi.org/10.1021/ef950227t

[9] T. Phan, A. R. Sane, B. Rego de Vasconcelos, A. Nzihou, P. Sharrock, D. Grouset, D. Pham Minh, *Appl. Catal., B* **2018**, *224*, 310. DOI: https://doi.org/10.1016/j.apcatb.2017.10.063

[10] J. W. Bae, J. H. Oh, K. W. Jun, Y. J. Lee, J.-H. Ko, S.-L. Song, K.-S. Min, *EP 2 371 799 A1*, **2011**.

[11] B. Rego de Vasconcelos, Phosphates-based catalysts for synthetic gas (syngas) production using CO_2 and CH_4, *Ph.D. Thesis*, École Nationale Supérieure des Mines d'Albi-Carmaux, Albi **2016**.

[12] M. Usman, W. M. A. Wan Daud, H. F. Abbas, *Renewable Sustainable Energy Rev.* **2015**, *45*, 710. DOI: https://doi.org/10.1016/j.rser.2015.02.026

[13] J. Newnham, K. Mantri, M. H. Amin, J. Tardio, S. K. Bhargava, *Int. J. Hydrogen Energy* **2012**, *37 (2)*, 1454. DOI: https://doi.org/10.1016/j.ijhydene.2011.10.036

[14] J.-H. Kim, D. J. Suh, T.-J. Park, K.-L. Kim, *Appl. Catal., A* **2000**, *197 (2)*, 191. DOI: https://doi.org/10.1016/S0926-860X(99)00487-1

[15] J. Zhang, H. Wang, A. K. Dalai, *Appl. Catal., A* **2008**, *339 (2)*, 121. DOI: https://doi.org/10.1016/j.apcata.2008.01.027

[16] A. G. Bhavani, W. Y. Kim, J. Y. Kim, J. S. Lee, *Appl. Catal., A* **2013**, *450*, 63. DOI: https://doi.org/10.1016/j.apcata.2012.10.008

[17] M. Jafarbegloo, A. Tarlani, A. Wahid Mesbah, S. Sahebdelfar, *Int. J. Hydrogen Energy* **2015**, *40 (6)*, 2445. DOI: https://doi.org/10.1016/j.ijhydene.2014.12.103

[18] R. Dębek, M. Radlik, M. Motak, M. E. Galvez, W. Turek, P. Da Costa, T. Grzybek, *Catal. Today* **2015**, *257 (P1)*, 59. DOI: https://doi.org/10.1016/j.cattod.2015.03.017

[19] L. Lloyd, in *Handbook of Industrial Catalysts* (ed: L. Lloyd), Springer, New York **2008**.

[20] C. E. Figueira, P. F. M. Junior, R. Giudici, R. M. B. Alves, M. Schmal, *Appl. Catal., A* **2018**, *550*, 297. DOI: https://doi.org/10.1016/j.apcata.2017.11.019

[21] W. Donphai, K. Faungnawakij, M. Chareonpanich, J. Limtrakul, *Appl. Catal., A* **2014**, *475 (5)*, 16. DOI: https://doi.org/10.1016/j.apcata.2014.01.014

Dry reforming of methane has been intensively studied during the last decade, but it is still not deployed on the industrial scale. One of the main challenges of the process is the development of an active and stable reforming catalyst. Hydroxyapatite is reported as a new promising material to design highly active and stable catalysts for this process.

A Comparative Study of Hydroxyapatite- and Alumina-Based Catalysts in Dry Reforming of Methane

B. Rego de Vasconcelos, D. Pham Minh*, E. Martins, A. Germeau, P. Sharrock, A. Nzihou

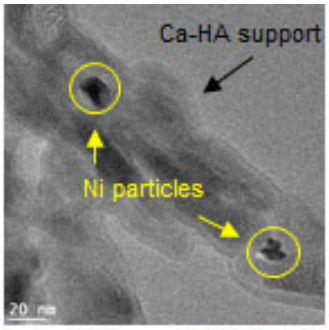

$$CH_4 + CO_2 \rightarrow 2CO + 2H_2$$